ROYAL SOCIETY
OF CHEMISTRY

COMMUNICATION

Check for updates

Resonant phonon modes induced by molecular rotations in α-pentaerythritol crystals†

Simin Wang, [a] Hongzhao Fan, [b] Zhe Zhang, [c] Liang Sun, [a] Jialu Chen, [b] Nuo Yang, [d] Yanguang Zhou, *[b] Bing Li*[c] and Liang Dai *[a]

Solid-state cooling employing barocaloric materials, especially plastic crystals, paves a promising way for eco-friendly refrigeration. However, inadequate understanding of the thermal properties hinders their practical applications. Here, we take α-pentaerythritol crystals as an example and reveal that the thermal transport is anisotropic, and the lattice dynamics is highly anharmonic. More importantly, we find that the two lowest-energy resonant phonon modes, associated with two mutually perpendicular molecular rotations, play critical roles in thermal conductivity and phase stability. The two optical modes suppress the acoustic branches by the avoided-crossing effect and hybridize with and strongly scatter acoustic phonons, further hindering thermal transport in α-pentaerythritol crystals. Furthermore, pressure can largely tune the rotational dynamics, reduce the resonance, and increase the phonon transmission and by adjusting the pressure from 0 MPa to 3500 MPa, an increase of 108% and 103% in in-plane and out-of-plane thermal conductivity, respectively, can be achieved. Our work provides a microscopic understanding of the rotational dynamics in α-pentaerythritol crystals, which can facilitate designing molecules to achieve a better barocaloric effect with more excellent thermal properties.

Introduction

Plastic crystals, such as neopentylglycol (NPG, $(CH_3)_2C(CH_2OH)_2$) and pentaerythritol (PE, $C(CH_2OH)_4$), are promising next-generation refrigerants due to their giant barocaloric effect.[1,2] Plastic crystals can undergo a disordered–ordered phase transition driven by a relatively low pressure and belong to phase change materials (PCMs).[3,4] Strikingly, plastic crystals with a barocaloric effect can exhibit entropy changes of up to several hundreds of joules per kilogram per Kelvin, comparable to commercial refrigerants.[1,2] Besides the barocaloric effect, the magnetocaloric effect (MCE),[5] electrocaloric effect (ECE),[6] and elastic caloric effect (eCE)[7] can also occur during solid–solid phase transitions in specific materials. However, their entropy changes are one to two orders of magnitude smaller than that of commercial refrigerants.[1,2] Therefore, barocaloric materials with the advantages of being environment-friendly, highly efficient, and cost-effective, are undoubtedly the best candidates for the next-generation solid-state refrigerants.

However, the thermal properties of plastic crystals, such as thermal transport and phase transitions, have not been fully understood on the fundamental level yet. For practical applications as refrigerants, it is known that the low thermal conductivity (commonly below 1 W m^{-1} K^{-1}) is one of the obstacles.[8,9] Curiously, to our best knowledge, none of the literature has focused on phonon transport in plastic crystals, even though low thermal transport has also been suggested as a critical challenge for their application as PCMs.[4,10] In particular, molecular reorientations are critical for the phase transitions of plastic crystals.[1,11,12] Meanwhile, experimental and theoretical studies show that the organic molecules' rotational or torsional dynamics in weakly interacted systems typically correspond to low-lying optical phonon modes.[13–15] It is known that interactions between low-frequency optical phonon modes and propagating modes,[16,17] especially the resonant effect featured by flat optical bands in the acoustic frequency range and quasi-localized hybridized acoustic modes,[18,19] significantly affect the thermal transport in the materials. However, how the rotational dynamics affects the phonon transport in the plastic crystal remains unknown. Furthermore, the lack of a phase transition mechanism usually associated with phonon collapse[20] hinders the design of new molecules to overcome the inherent drawbacks of plastic

[a] Department of Physics, City University of Hong Kong, Kowloon 999077, Hong Kong, China. E-mail: liangdai@cityu.edu.hk

[b] Department of Mechanical and Aerospace Engineering, Hong Kong University of Science and Technology, Clear Water Bay 999077, Hong Kong, China. E-mail: maeygzhou@ust.hk

[c] Shenyang National Laboratory (SYNL) for Materials Science, Institute of Metal Research, Chinese Academy of Sciences, Shenyang 110016, China. E-mail: bingli@imr.ac.cn

[d] School of Energy and Power Engineering, Huazhong University of Science and Technology, Wuhan 430074, China

† Electronic supplementary information (ESI) available. See DOI: https://doi.org/10.1039/d2tc02878f

This journal is © The Royal Society of Chemistry 2022

J. Mater. Chem. C, 2022, **10**, 14431–14438 | **14431**

crystals, such as thermal hysteresis.[1] Therefore, in-depth studies on phonon properties are urgently needed and detailed microscopic mechanisms are of great significance for better understanding and optimizing the thermal properties of plastic crystals.

In this work, we thoroughly investigate the atomic dynamics in α-PE crystals using molecular dynamics (MD) simulations and density-functional theory (DFT) calculations. The thermal conductivity is anisotropic and the lattice dynamics is highly anharmonic. More strikingly, we find that two resonant phonon modes, stemming from the rotations of the molecules, play vital roles in the thermal transport and phase stability of α-PE. The corresponding optical phonon modes not only suppress the acoustic phonon modes by the anti-crossing effect but also hybridize with and strongly scatter acoustic modes and we further observe that changes in pressure lead to shifts of the low-lying optical branches, thereby tuning the rotational dynamics, reducing the resonance, enhancing the phonon transmission, and significantly increasing the thermal conductivity by a factor of 1.

Results and discussion

At temperatures lower than ∼459 K, pentaerythritol crystallizes in the α phase or the ordered phase in which molecules exhibit preferred orientations with space group *I*-4.[21] The lattice structure was obtained from the experiments,[21] as shown in Fig. 1. Obviously, the α-PE crystal has a layered configuration: on the *ab*-plane, the molecules are connected by hydrogen bonds; while between layers, *i.e.*, along the *c*-axis, they are bound together mainly by van der Waals interactions, which is demonstrated by energy between layers as a function of layer spacing, as shown in Fig. S1 (ESI†). The difference in interactions along different directions leads to anisotropic heat transport in α-PE, which will be described later.

Thermal conductivity

We performed all molecular dynamics (MD) simulations using the LAMMPS[22] program with a time step of 0.5 fs. The GROMOS force field[23] was adopted to model PE molecules. To verify the accuracy of the force field, the heat capacity was computed by integrating the product of phonon density of states (PDOS) and Bose–Einstein distribution,[24] and it is in good agreement with experimental data in the temperature range of 275–450 K, as shown in Fig. S2 (ESI†). After respective relaxation in the *NPT*, *NVT*, and *NVE* ensembles for 1 ns successively, heat current was collected every eight time steps for 0.5 ns, and Green–Kubo equilibrium molecular dynamics (GK-EMD)[25] was applied to compute the thermal conductivity κ in the *NVE* ensemble:

$$\kappa_{ij} = \frac{1}{k_B T^2 V} \int_0^t J_i(0) J_j(\tau) \mathrm{d}\tau$$

in which subscript i and j represent different directions, k_B is the Boltzmann constant, and T and V are temperature and volume, respectively. The brackets $\langle \rangle$ denote the ensemble average, and J_i is the heat current in the i direction. To obtain the convergent thermal conductivity, 40 independent GK-EMD simulations with an autocorrelation time of 50 ps were conducted, as shown in Fig. S3 (ESI†), and the statistical errors in Fig. 2 are standard deviations.

Thermal conductivities at different temperatures were calculated, as shown in Fig. 2(a), and the average thermal conductivity $(\frac{1}{2}(\kappa_{ab} + \kappa_c))$ is in good agreement with the experiment.[26] The anisotropy of in-plane and out-of-plane thermal conductivities is apparent. The in-plane thermal conductivity is 3-fold the out-of-plane thermal conductivity, which can be attributed to the strength of in-plane hydrogen bonds being stronger than the out-of-plane van der Waals interactions.[27–30] Moreover, the weak interlayer interactions also lead to easily tunable layer spacing and phonon group velocity (the slope of longitudinal acoustic branches along the *Γ*–*M* direction, as shown in Fig. S7, ESI†) and thus the dependence of thermal conductivity on out-of-plane expansion is exponential, as shown in Fig. S4 (ESI†).[31]

Furthermore, as shown in Fig. 2(a), the thermal conductivity evaluated using GK-EMD roughly obeys a temperature-dependency of $T^{-0.46}$, which seriously deviates from the typical T^{-1} relationship. It is known that thermal conductivities of weakly anharmonic solids, which are dominated by three-phonon scattering, follow a T^{-1} dependency.[32] Actually, the temperature dependency here is
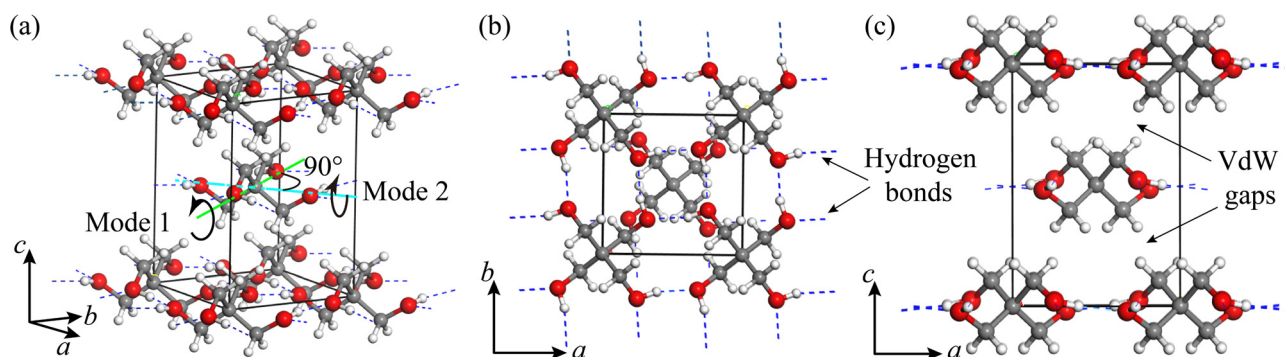

Fig. 1 Perspective (a), top (b), and lateral (c) views of the α-PE conventional cell. H, C, and O atoms are shown in white, gray, and red, respectively, and the blue dashed lines are hydrogen bonds. The molecules are connected by hydrogen bonds forming the layers on the *ab*-plane (b), while the dominant interaction between the layers (c) is the van der Waals interaction. A schematic diagram of the two rotational motions mutually perpendicular corresponding to the two lowest-energy resonant optical modes at the *Γ* point is shown in (a), with their axes in green and cyan, respectively, and the high-symmetric path *Γ*–*X* coincides with the axis of mode 1. For simplicity, the phonon modes are only depicted on the central molecule of the unit cell.

14432 | *J. Mater. Chem. C*, 2022, **10**, 14431–14438

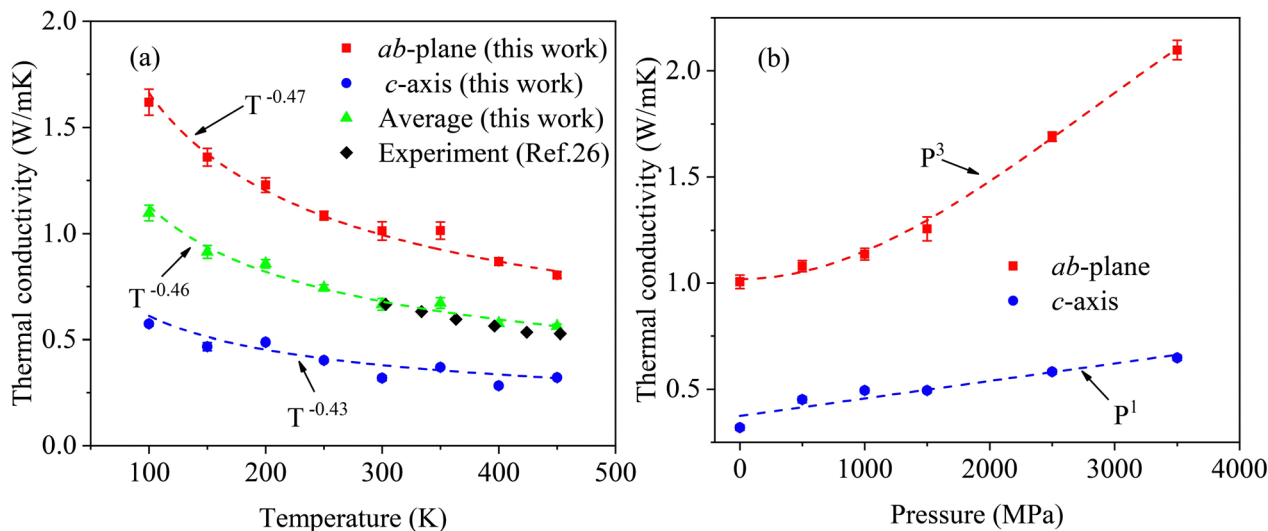This journal is © The Royal Society of Chemistry 2022

Fig. 2 Temperature (a) and pressure (b) dependency of thermal conductivity of α-PE crystals evaluated with GK-EMD and experimentally. The average thermal conductivities (green triangles) match well with the experimental data (black diamonds in (a)) in ref.26 in the temperature range from 300 to 450 K. The theoretical thermal conductivities were exponentially fitted from 100 to 450 K. In (b), the calculated thermal conductivity increases with pressure by a factor of 1 from 0 MPa to 3500 MPa at 300 K.

close to those of other complex crystals where temperature-induced renormalization of the phonons is significant.[20] Thus, the α-PE crystal is highly anharmonic.[20,33] As an indication of lattice harmonicity, Grüneisen parameter γ is also proportional to dP/dT. Therefore, according to the Clausius–Clapeyron relation, more anharmonic materials have more considerable entropy changes.[1] As mentioned above, plastic crystals exhibit a giant barocaloric effect, while they also have low thermal conductivities, which is consistent with the discussions here.

To solve this contradiction, two strategies can be adopted. One is to improve the thermal transport of plastic crystals directly. Our calculations, shown in Fig. 2(b), demonstrate that when the pressure increases from 0 to 3500 MPa, the in-plane and out-of-plane thermal conductivities follow P^3 and P^1 dependency and increase by around 108.5% and 103.2%, respectively.[9] This can be attributed to the suppression of rotational dynamics by pressure, reducing the resonance between the propagating modes and optical modes, thereby enhancing the phonon transmission and thermal conductivity. In addition, compositing plastic crystals with other components with high thermal conductivity, such as graphite, could significantly enhance heat transfer.[10]

Resonant phonon modes

To further understand the thermal transport in α-PE, the vibrational properties were investigated under the harmonic approximation *via* the finite displacement method implemented using VASP[34] combined with Phonopy[35] (see ESI† for details). The static harmonic phonon dispersions along selected high-symmetric paths of the primitive cell are shown in Fig. 3(a)–(d) and the complete phonon dispersions are shown in Fig. S5 (ESI†). It is seen that the acoustic phonon branches are remarkably suppressed by the optical phonon branches around 2 THz in the Γ–X, Γ–N, and Γ–S_0 directions and the avoided-crossing or anti-crossing[15,36–40] between the lowest-energy optical phonon band and longitudinal acoustic

(LA) phonon band persists for more than half of the Brillouin zone. In addition, the sizeable gap between the flat bands indicates a remarkably high coupling strength or hybridization between optical and acoustic modes,[40] whereas in the Γ–M direction, the LA branch overlaps the lowest optical branch directly, again indicating the dramatic interaction between the optical and acoustic modes.

While the avoided-crossing involving acoustic and optical phonon branches is widely found in phonon-glass thermoelectric materials with cage-like or layered frames,[36–38] this phenomenon is not ordinary in an organic crystal. In phonon-glass thermoelectric materials with cage-like or layered frames, the heavy metal atoms fill the lattice voids or interlayer gaps. However, in the α-PE crystal, there are no such rattles. To understand the nature of the two low-lying optical modes around 2 THz, we visualized the modes by eigenvectors.[38,40] For the lowest-lying optical mode of 2.43 THz at the Γ point, we can see that the atoms in a PE molecule rotate around an O–C–O axis, as shown in Supplementary Movie 1 (ESI†). The axis is along the Γ–X direction and is marked in green in Fig. 1(a) in the conventional cell. The rotational axis is on the *ab*-plane, *i.e.*, the hydrogen bond network plane, while the molecule's rotation is perpendicular to the plane. Similarly, the second-lowest optical mode of 2.43 THz at the Γ point recorded in Supplementary Movie 2 (ESI†) is also a rotational motion, while its axis (marked in cyan in Fig. 1(a)) is another O–C–O axis, perpendicular to the axis of the lowest-lying optical mode. Thus, the flat bands are induced by two mutually perpendicular rotations of molecules. The rotations are symmetrical due to the spherical shape of the PE molecule,[41] hence forming closed eigenvector loops. Correspondingly, two peaks at 2.15 and 2.25 THz are observed in the Raman spectrum at 300K, highlighted in Fig. S6 (ESI†), verifying the calculations.

The hybridized modes at the Brillion zone boundary, *i.e.*, $q = 0.5$, are recorded in Supplementary Movies 3 and 4 (ESI†). For the 1.79 THz mode, the vibrations remain perpendicular to
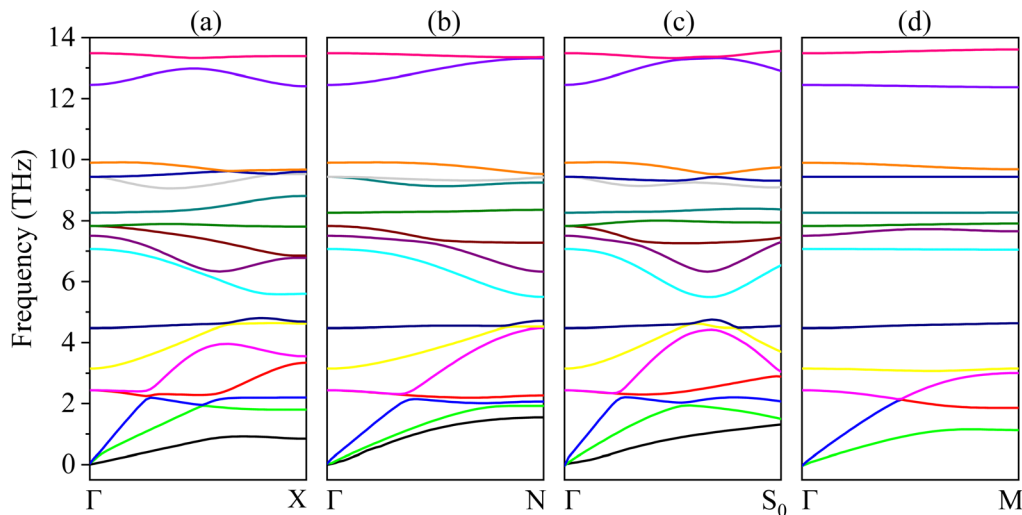
This journal is © The Royal Society of Chemistry 2022

J. Mater. Chem. C, 2022, **10**, 14431–14438 | **14433**

Fig. 3 Phonon dispersions calculated by the finite displacement method along the $\Gamma-X$ (a), $\Gamma-N$ (b), $\Gamma-S_0$ (c), and $\Gamma-M$ (d) directions. The $\Gamma-X$ path is on the ab-plane and along the axis of mode 1, as shown in Fig. 1(a) and the path $\Gamma-M$ is along the c-axis. The avoided-crossing between the lowest optical phonon branch and the LA branch is remarkable in (a), (b), and (c). The LA branch (blue line) overlaps the optical branch (red line) in (d).

the high-symmetric path, which follows the feature of the transverse acoustic (TA2) mode. However, in Supplementary Movie 3 (ESI†), we can still identify the rotational motions around the axis along the $\Gamma-X$ direction, similar to the motions observed in Supplementary Movie 1 (ESI†), even though the phase difference of the motions is evident for the hybridized mode. The hybridization between the second-lowest optical bands with LA mode is vigorous at 2.16 THz. The atomic motion becomes utterly perpendicular to the $\Gamma-X$ direction, as shown in Supplementary Movie 4 (ESI†), resulting in a zero phonon group velocity and a quasi-localized acoustic band on the spectrum. Thus, because of the different rotational motions at the Γ point, the lowest and second-lowest optical branches are hybridized with the TA2 and LA acoustic branches, respectively.

It is worth noting that the resonance induced by molecular rotations in the α-PE crystal differs from the standing wave in the branched silicon nanowires.[39,40,42] In the latter, there is no such rotational motion and the standing wave is induced by the total reflection of waves at the end of symmetrical branches. Similarly, heavy guests in phonon-glass thermoelectric materials vibrate independently and the wave can be reflected between the guests,[37] indicating the localized nature of the vibrations in the flat bands. The essential difference between the above three mechanisms is reflected by the motions of low-lying optical phonon modes at the Γ point. In the α-PE crystal, the symmetrical molecular rotations at the Γ point form closed eigenvector loops, resulting in standing waves, while in the phonon-glass thermoelectric materials, the opposite translational vectors of the guest and host atoms at the Γ point cancel each other out.[37]

Undoubtedly, the interactions and hybridizations between optical and acoustic modes at low frequencies significantly affect the properties of the α-PE crystal. To investigate the effect on thermal transport, the non-equilibrium molecular dynamics (NEMD) simulations were performed and the phonon transmission coefficient $PT(\omega)$ was calculated by the frequency domain direct

decomposition method (FDDDM) combined with Landauer theory:[43,44]

$$PT(\omega) = \frac{1}{k_B \Delta T} \sum_{i \in L} \sum_{j \in R} \mathrm{Re}\left[\int_{-\infty}^{+\infty}\left\langle \left.\frac{\partial U_j}{\partial \vec{r}_{ij}}\right|_{\tau} \vec{v}_i(0) - \left.\frac{\partial U_i}{\partial \vec{r}_{ij}}\right|_{\tau} \vec{v}_j(0) \right\rangle \mathrm{e}^{-i\omega\tau}\mathrm{d}\tau\right]$$

where ΔT refers to the temperature difference between the left and the right thermostats and U and $\vec{v}$ are the interatomic potential energy and velocity of the atom, respectively and $\vec{r}_{ij}$ denotes the distance between atom i and atom j. In the NEMD simulations, the hot and cold thermostats were applied next to the two fixed ends, with a temperature difference of 60 K and a distance of 11.8 nm. The trajectories of atomic velocities were output every eight time steps to calculate the phonon transmission after the heat current and the temperature gradient were stable. For comparison, the ballistic transmission coefficient is also shown in Fig. 4(a). The transport length was set as 0.6 nm when calculating the ballistic transmission coefficient, which is short enough to ensure that all the phonons are transported ballistically.

The $PT(\omega)$ reported in Fig. 4(a) demonstrates that at 300 K, phonons below 2 THz have a higher phonon transmission coefficient because low-frequency phonons have a longer wavelength.[45] The transport is close to the ballistic transport below 1.65 THz. However, the abrupt drop in the phonon transmission after the turning point at 1.65 THz suggests that the interactions between acoustic branches and low-lying optical branches are pretty strong even far from 2 THz. Furthermore, as shown in Fig. 4(a), the phonon transmission calculated at different temperatures demonstrates that not only the intensity of the peaks decreases, but also the positions of the peaks shift as the temperature increases from 200 to 400 K. These collapses and shifts indicate the high anharmonicity in the α-PE crystal, leading to a $T^{-0.46}$ temperature-dependency of thermal conductivity, as shown in Fig. 2(a). Among the peaks, the first peak collapses and shifts to a lower frequency apparently as the
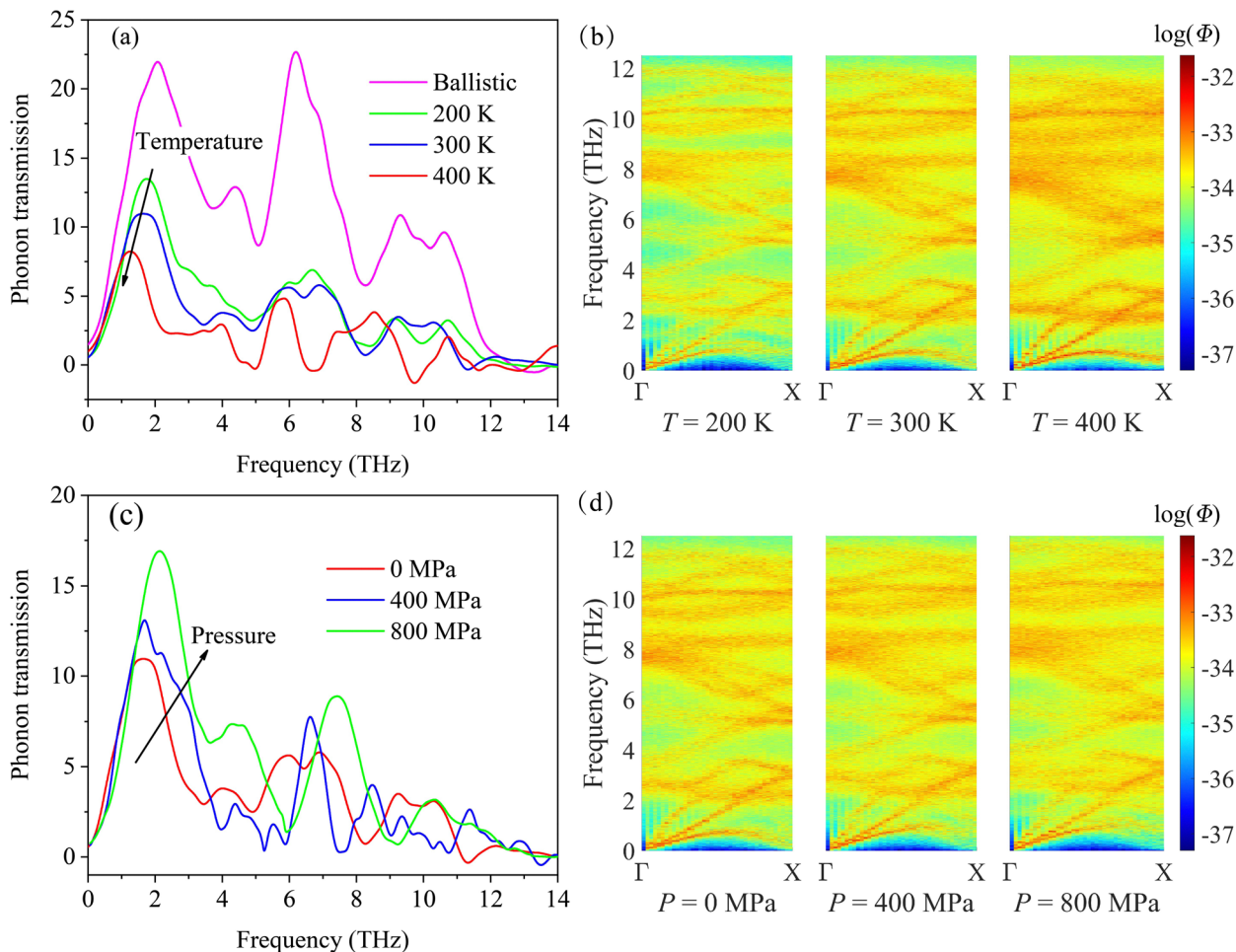
14434 | *J. Mater. Chem. C*, 2022, **10**, 14431–14438

This journal is © The Royal Society of Chemistry 2022

Fig. 4 Frequency-dependent transmission coefficients calculated by the frequency-dependent direct decomposed method (FDDDM) in the frequency range of 0–14 THz at different temperatures (a) and pressures (c). Phonon dispersions computed by the spectral energy density (SED) method at different temperatures (b) and pressures (d) with a resolution of 0.025 × 0.005 THz.

temperature increases, which could be attributed to the softening of phonons. Hence, here, the role of the low-lying optical phonon in thermal transport becomes clear. The low-lying optical branches suppress the acoustic branches by the avoided-crossing effect, as shown in Fig. 3(a)–(c), which causes the acoustic phonon group velocity to drop dramatically to zero around 2 THz.[37,39,40] Furthermore, the anharmonic hybridizations between the acoustic and optical phonon modes span an extensive frequency range and inevitably scatter phonons, reducing the portion of heat transferred by acoustic phonons further.[14,38,46,47]

In addition to the shifts of peaks of the phonon transmission coefficient, the temperature-dependent phonon dispersions calculated by the spectral energy density (SED) method[48] also show the renormalization of phonons. The SED analysis, which is the function of wave vector q and the frequency ω, was performed using the EMD simulations and calculated by projecting the atomic velocity in the crystal onto the normal modes of vibration:[48]

$$\Phi(\boldsymbol{q}, \omega) = \frac{1}{4\pi\tau_0} \sum_{\alpha}^{3} \sum_{b}^{N_a} \frac{m_b}{N_u} \left| \sum_{l}^{N_u} \int_{0}^{\tau_0} v_{\alpha,b,l}(\tau) e^{i\boldsymbol{q}\cdot r_0^l} e^{-i\omega\tau} d\tau \right|^2$$

in which τ_0 is the total time to collect the velocity of atoms, m_b is the mass of the bth atom, and r_0^l is the equilibrium position of the lth unit cell and N_a and N_u are the number of atomic types and total unit cells, respectively. $v_{\alpha,b,l}(\tau)$ is the velocity of the bth atom in the lth unit cell along the α (x, y, z) direction at time τ.

The phonon dispersion calculated by the finite displacement method is within the harmonic approximation, while the results of the SED method can contain anharmonicity. To check the consistency of the two methods, the phonon dispersions along the Γ–X and Γ–M paths are plotted in Fig. 5 for comparison. It is seen that the phonon dispersions calculated by the SED method at 10 K and VASP at 0 K are in reasonable agreement. Overall, the reasonable agreement between phonon dispersions calculated by the two different methods indicates that our calculations based on molecular dynamics simulations should be physically meaningful. The phonon dispersions at different temperatures are plotted in Fig. 4(b). It is seen that the lines throughout the spectra become more blurred, indicating the increased scattering between phonons and the decreased phonon lifetimes when the temperature increases from 200 to 400 K.[49] In addition to being broader, the lines between 2 and
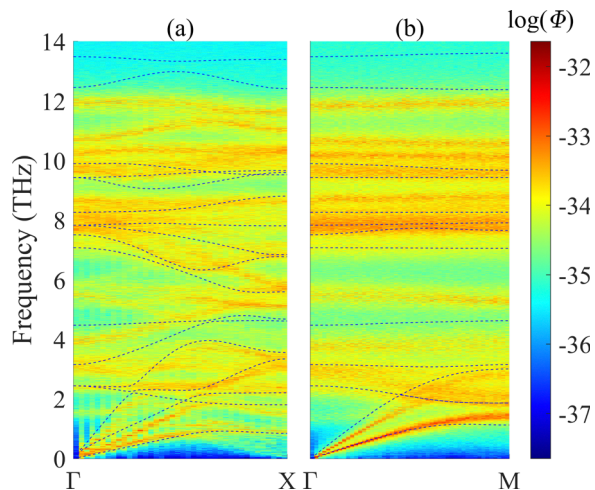
This journal is © The Royal Society of Chemistry 2022

J. Mater. Chem. C, 2022, **10**, 14431–14438 | **14435**

Fig. 5 Comparison of phonon dispersion calculated by DFT and MD along $\Gamma - X$ (a) and $\Gamma - M$ (b) paths. Blue dashed lines are DFT results (finite displacement method) and the contour map is the MD result (SED method) at 10 K.

4 THz are significantly shifted compared to lines in other frequency ranges, especially from 200 to 300 K. These shifts manifest the large anharmonicity of phonons in this frequency range.[13,38,50,51] Thus, unavoidably, these phonons interact with acoustic phonons and scatter them strongly, consistent with the discussions above.

Effect of pressure

As mentioned above, the high thermal conductivity of plastic crystals is necessary for their applications as refrigerants and PCMs. Therefore, enhancing phonon transport becomes critical. The results in Fig. 2(b) show that when the pressure is increased from 0 to 3500 MPa, the in-plane and out-of-plane thermal conductivities increase substantially from 1.0 and 0.32 W m^{-1} K^{-1} to 2.1 and 0.65 W m^{-1} K^{-1}, respectively. To figure out the reasons, phonon transmission and phonon dispersions were calculated. As seen from Fig. 4(c), the peaks around 2 THz shift to a higher frequency after applying pressure and phonon transmission increases significantly. This suggests that high pressures can reduce the resonance between the optical and acoustic phonon modes, leading to a significant increase in thermal transport.

It is also known that the pressure plays a vital role in the phase transition of plastic crystals.[1,11] As observed in Fig. 4(b), when the temperature increases from 200 K to 400 K, the second lowest-energy branch moves significantly downward, and the two lowest-energy optical branches gradually merge. As mentioned above, the two lowest-energy phonon modes correspond to two mutually perpendicular rotational motions. Therefore, the phase
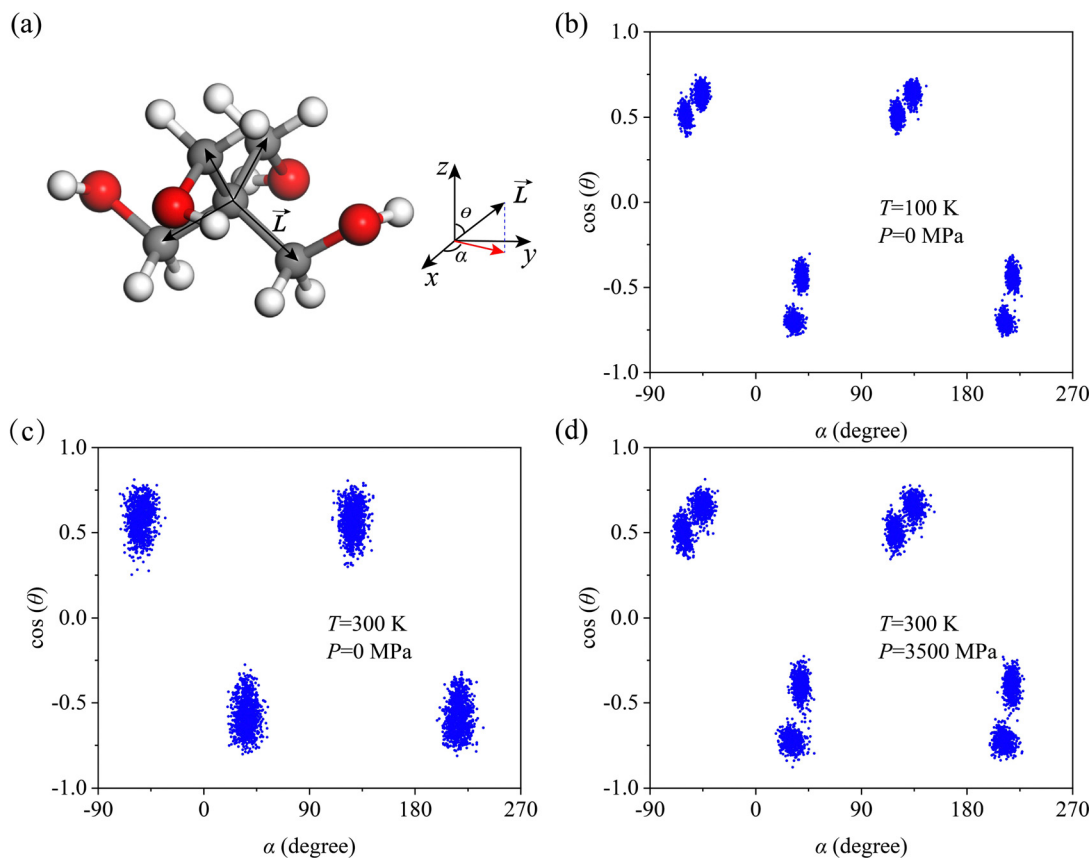

Fig. 6 Orientations of molecules in the α-PE crystal. The directions of molecules are defined by angles α and θ in (a). The eight clusters in (b) represent two orientations of molecules at 0 MPa and 100 K. Comparing the distributions in (c) and (d), the reorientations of molecules are significantly suppressed by the pressure at 300 K.

14436 | *J. Mater. Chem. C*, 2022, **10**, 14431–14438

This journal is © The Royal Society of Chemistry 2022

becomes unstable as the temperature increases, while the two motions become more isotropic. The shifts of the lowest-lying phonon branches are also observed when strain or stress perpendicular to the hydrogen bond network is applied, as shown in Fig. S7 (ESI†). Identical with the Γ–X path, among optical branches, only the two lowest optical phonon branches shift significantly as the strain or stress changes along the Γ–M path. This is attributed to overlaps of optical modes and acoustic modes, as shown in Fig. 3(d). On the other hand, the critical role of the low-lying optical branches in the phase stability is again illustrated. The pressure-dependent phonon dispersions of the α-PE crystal are plotted in Fig. 4(d). It can be seen that as the pressure increases from 0 to 800 MPa, remarkably, the two lowest optical branches separate. Therefore, we can conclude that high pressure and low temperature stabilize the α-PE crystal by hindering the isotropy or degeneration of the two lowest rotational phonon modes. Meanwhile, the hybridizations of optical and propagation modes are reduced due to the upward movement of the optical branches, consistent with the discussions above.

To further elucidate the effect of pressure on molecular rotations, we defined four vectors, pointing from the center carbon atom to carbon atoms in a methanol group and the orientations of molecules indicated by angle α and θ, as illustrated in Fig. 6(a). Obviously, after a 1 ns equilibrium MD simulation, two molecular directions appear at 0 MPa and 100 K, while at 300 K, the eight spots merge into four ellipses due to the intensive thermal fluctuation and volume expansion, indicating a reorientation process of the molecules from 100 K to 300 K. Then, applying a pressure of 3500 MPa, it is strikingly seen in Fig. 6(d) that the eight clusters separate again at 300 K and the distributions are similar to those at 0 MPa and 100 K in Fig. 6(b). Therefore, the pressure can suppress the rotations of the individual molecule and enhance the energy barrier of rotations,[1,11] thereby stabilizing the low-entropy phase. In summary, the pressure can effectively suppress the collective and individual molecular rotational dynamics, stabilizing the phase, reducing the phonon scattering, and significantly increasing the thermal transport.

Conclusions

In summary, we observed that the two lowest-energy optical phonon modes play a crucial role in the thermal transport and phase stability of the α-PE crystal. The two modes were proven to be resonant modes induced by two mutually perpendicular rotational motions, which have been observed for the first time in bulk crystals. These two optical phonon branches suppress the acoustic phonon modes by the avoided-crossing effect. In addition, the lowest and the second-lowest optical phonon modes are significantly hybridized with transverse (TA2) and longitudinal (LA) phonon modes, respectively. Meanwhile, the two lowest-energy optical phonon modes are highly anharmonic and thus strongly scatter the acoustic phonons, hindering the thermal transport in the α-PE crystal. However, the rotational dynamics can be suppressed by pressure, which stabilizes the phase, reduces the hybridization or resonance between acoustics and optical phonon modes, and increases phonon transmission around 2 THz, resulting in a significant increase in thermal conductivity. The insights provided by our work into the atomic dynamics of the α-PE crystal may facilitate the understanding and optimization of the properties of barocaloric materials. Furthermore, the molecular rotations that we discovered in this work are a novel mechanism for inducing the resonance, enriching the knowledge of resonance, and benefiting the thermal management of materials.

Conflicts of interest

There are no conflicts to declare.

Acknowledgements

References

1 B. Li, Y. Kawakita, S. Ohira-Kawamura, T. Sugahara, H. Wang, J. Wang, Y. Chen, S. I. Kawaguchi, S. Kawaguchi, K. Ohara, K. Li, D. Yu, R. Mole, T. Hattori, T. Kikuchi, S. Ichiro Yano, Z. Zhang, Z. Zhang, W. Ren, S. Lin, O. Sakata, K. Nakajima and Z. Zhang, *Nature*, 2019, **567**, 506–510.

2 P. Lloveras, A. Aznar, M. Barrio, P. Negrier, C. Popescu, A. Planes, L. Mañosa, E. Stern-Taulats, A. Avramenko, N. D. Mathur, X. Moya and J. L. Tamarit, *Nat. Commun.*, 2019, **10**, 1–7.

3 M. Barrio, J. Font, J. Muntasell, J. Navarro and J. L. Tamarit, *Sol. Energy Mater.*, 1988, **18**, 109–115.

4 A. Fallahi, G. Guldentops, M. Tao, S. Granados-Focil and S. Van Dessel, *Appl. Therm. Eng.*, 2017, **127**, 1427–1441.

5 V. K. Pecharsky and K. A. Gschneidner Jr, *Phys. Rev. Lett.*, 1997, **78**, 4494–4497.

6 A. S. Mischenko, Q. Zhang, J. F. Scott, R. W. Whatmore and N. D. Mathur, *Science*, 2006, **311**, 1270–1271.

7 L. Mañosa and A. Planes, *Adv. Mater.*, 2017, **29**, 1603607.

8 P. Lloveras and J.-L. Tamarit, *MRS Energy Sustainability*, 2021, **8**, 3–15.

9 A. Aznar, P. Negrier, A. Planes, L. Mañosa, E. Stern-Taulats, X. Moya, M. Barrio, J. L. Tamarit and P. Lloveras, *Appl. Mater. Today*, 2021, **23**, 101023.

10 X. Wang, Q. Guo, Y. Zhong, X. Wei and L. Liu, *Renewable Energy*, 2013, **51**, 241–246.

11 F. B. Li, M. Li, X. Xu, Z. C. Yang, H. Xu, C. K. Jia, K. Li, J. He, B. Li and H. Wang, *Nat. Commun.*, 2020, **11**, 1–8.

12 S. Das, A. Mondal and C. M. Reddy, *Chem. Soc. Rev.*, 2020, **49**, 8878–8896.

13 T. Hata, G. Giorgi and K. Yamashita, *Nano Lett.*, 2016, **16**, 2749–2753.

14 Z. Zhang, Y. Ouyang, Y. Guo, T. Nakayama, M. Nomura, S. Volz and J. Chen, *Phys. Rev. B*, 2020, **102**, 195302.

15 E. Garlatti, L. Tesi, A. Lunghi, M. Atzori, D. J. Voneshen, P. Santini, S. Sanvito, T. Guidi, R. Sessoli and S. Carretta, *Nat. Commun.*, 2020, **11**, 1–10.

16 D. Ma, X. Wan and N. Yang, *Phys. Rev. B*, 2018, **98**, 1–5.

17 H. Ma, C. Li, Y. Ma, H. Wang, Z. W. Rouse, Z. Zhang, C. Slebodnick, A. Alatas, S. P. Baker, J. J. Urban and Z. Tian, *Phys. Rev. Lett.*, 2019, **123**, 155901.

18 E. S. Toberer, A. Zevalkink and G. J. Snyder, *J. Mater. Chem.*, 2011, **21**, 15843–15852.

19 J. Yang, W. Zhang, S. Q. Bai, Z. Mei and L. D. Chen, *Appl. Phys. Lett.*, 2007, **90**, 10–13.

20 J. Klarbring, O. Hellman, I. A. Abrikosov and S. I. Simak, *Phys. Rev. Lett.*, 2020, **125**, 45701.

21 Q. Zhou, T. Yang, Z. Zhong, F. Kausar, Z. Wang, Y. Zhang and W. Z. Yuan, *Chem. Sci.*, 2020, **11**, 2926–2933.

22 S. Plimpton, *J. Comput. Phys.*, 1995, **117**, 1–19.

23 M. Stroet, B. Caron, K. M. Visscher, D. P. Geerke, A. K. Malde and A. E. Mark, *J. Chem. Theory Comput.*, 2018, **14**, 5834–5845.

24 P. Roedhammer, W. Weber, E. Gmelin and K. H. Rieder, *J. Chem. Phys.*, 1976, **64**, 581–585.

25 R. Kubo, *Rep. Prog. Phys.*, 1966, **29**, 255–284.

26 B. Feng, J. Tu, J.-W. Sun, L.-W. Fan and Y. Zeng, *Int. J. Heat Mass Transfer*, 2019, **141**, 789–798.

27 C. Li, H. Ma, T. Li, J. Dai, M. A. J. Rasel, A. Mattoni, A. Alatas, M. G. Thomas, Z. W. Rouse, A. Shragai, S. P. Baker, B. J. Ramshaw, J. P. Feser, D. B. Mitzi and Z. Tian, *Nano Lett.*, 2021, **21**, 3708–3714.

28 X. Yu, R. Li, T. Shiga, L. Feng, M. An, L. Zhang, J. Shiomi and N. Yang, *J. Phys. Chem. C*, 2019, **123**, 26735–26741.

29 S. Deng, D. Ma, G. Zhang and N. Yang, *J. Mater. Chem. A*, 2021, **9**, 24472–24479.

30 S. Wang, L. Sun, B. Li and L. Dai, *J. Phys. Chem. C*, 2021, **125**, 15853–15862.

31 P. Erhart, P. Hyldgaard and D. O. Lindroth, *Chem. Mater.*, 2015, **27**, 5511–5518.

32 M. Wu, Enamullah and L. Huang, *Phys. Rev. B*, 2019, **100**, 1–9.

33 Y. Zhou, Y. Xu, Y. Gao and S. Volz, *Phys. Rev. Mater.*, 2022, **6**, 1–9.

34 G. Kresse and J. Furthmüller, *Comput. Mater. Sci.*, 1996, **6**, 15–50.

35 A. Togo and I. Tanaka, *Scr. Mater.*, 2015, **108**, 1–5.

36 C. H. Lee, I. Hase, H. Sugawara, H. Yoshizawa and H. Sato, *J. Phys. Soc. Jpn.*, 2006, **75**, 1–5.

37 M. Christensen, A. B. Abrahamsen, N. B. Christensen, F. Juranyi, N. H. Andersen, K. Lefmann, J. Andreasson, C. R. H. Bahl and B. B. Iversen, *Nat. Mater.*, 2008, **7**, 811–815.

38 J. Qi, B. Dong, Z. Zhang, Z. Zhang, Y. Chen, Q. Zhang, S. Danilkin, X. Chen, J. He, L. Fu, X. Jiang, G. Chai, S. Hiroi, K. Ohara, Z. Zhang, W. Ren, T. Yang, J. Zhou, S. Osami, J. He, D. Yu, B. Li and Z. Zhang, *Nat. Commun.*, 2020, **11**, 1–8.

39 B. L. Davis and M. I. Hussein, *Phys. Rev. Lett.*, 2014, **112**, 055505.

40 S. Xiong, K. Sääskilahti, Y. A. Kosevich, H. Han, D. Donadio and S. Volz, *Phys. Rev. Lett.*, 2016, **117**, 1–6.

41 J. L. Tamarit, B. Legendre and J. M. Buisine, *Mol. Cryst. Liq. Cryst. Sci. Technol., Sect. A*, 1994, **250**, 347–358.

42 H. Honarvar and M. I. Hussein, *Phys. Rev. B*, 2016, **93**, 1–5.

43 Y. Zhou and M. Hu, *Phys. Rev. B: Condens. Matter Mater. Phys.*, 2015, **92**, 195205.

44 Y. Zhou and M. Hu, *Phys. Rev. B*, 2017, **95**, 115313.

45 W. Ren, Y. Ouyang, P. Jiang, C. Yu, J. He and J. Chen, *Nano Lett.*, 2021, **21**, 2634–2641.

46 J. He, M. Amsler, Y. Xia, S. S. Naghavi, V. I. Hegde, S. Hao, S. Goedecker, V. Ozoliņš and C. Wolverton, *Phys. Rev. Lett.*, 2016, **117**, 1–6.

47 S. S. Naghavi, J. He, Y. Xia and C. Wolverton, *Chem. Mater.*, 2018, **30**, 5639–5647.

48 J. A. Thomas, J. E. Turney, R. M. Iutzi, C. H. Amon and A. J. H. McGaughey, *Phys. Rev. B: Condens. Matter Mater. Phys.*, 2010, **81**, 81411.

49 S. Srinivasan and G. Balasubramanian, *Langmuir*, 2018, **34**, 3326–3335.

50 X. Wang, Y. Hong, D. Ma and J. Zhang, *J. Mater. Chem. C*, 2017, **5**, 5119–5127.

51 X. Li, P. F. Liu, E. Zhao, Z. Zhang, T. Guidi, M. D. Le, M. Avdeev, K. Ikeda, T. Otomo, M. Kofu, K. Nakajima, J. Chen, L. He, Y. Ren, X. L. Wang, B. T. Wang, Z. Ren, H. Zhao and F. Wang, *Nat. Commun.*, 2020, **11**, 1–9.